Laser Phys. Lett. **5**, No. 7, 532–542 (2008) / **DOI** 10.1002/lapl.200810032

Abstract: We report the experimental investigation of nonlinear cascaded lasing $\chi^{(3)} \leftrightarrow \chi^{(2)}$ effects in UV and visible ranges and high-order Stokes and anti-Stokes generation covering spectral space of about 18000 cm^{-1} by stimulated Raman scattering and multi-wave mixing processes under one-micron picosecond pumping in the paraelectric state of $NH_4H_2PO_4$ and $ND_4D_2PO_4$ single crystals. All recorded Raman induced laser wavelengths are identified and attributed to their SRS-promoting vibration modes. Brief review of nonlinear-laser processes in non-centrosymmetric phosphates of KH_2PO_4-family and some physical properties of $NH_4H_2PO_4$ and $ND_4D_2PO_4$ are given as well.

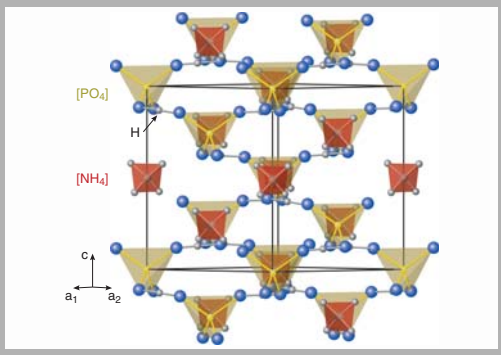

Plot of the crystal structure of $NH_4H_2PO_4$

Nonlinear-laser effects in $NH_4H_2PO_4$ (ADP) and $ND_4D_2PO_4$ (DADP) single crystals: almost two-octave multi-wavelength Stokes and anti-Stokes combs, cascaded lasing in UV and visible ranges with the involving of the second and third harmonic generation

A.A. Kaminskii, [1,*] *V.V. Dolbinina,* [1] *H. Rhee,* [2] *H.J. Eichler,* [2] *K. Ueda,* [3] *K. Takaichi,* [3] *A. Shirakawa,* [3] *M. Tokurakawa,* [3] *J. Dong,* [4] *and D. Jaque* [5]

[1] Institute of Crystallography, Russian Academy of Sciences, Moscow 119333, Russia
[2] Institute of Optics and Atomic Physics, Technical University of Berlin, Berlin 10623, Germany
[3] Institute for Laser Science, University of Electro-Communications, Tokyo 182-8585, Japan
[4] Department of Physics, School of Engineering and Physical Sciences, Heriot-Watt University, Edinburgh, EH14 4AS, UK
[5] Facultad de Ciencias, Universidad Autonoma de Madrid, Madrid 28049, Spain

Received: 24 March 2008, Accepted: 28 March 2008
Published online: 11 April 2008

Key words: Raman crystal; nonlinear-laser cascaded effects; stimulated Raman scattering; SHG; THG; Stokes and anti-Stokes comb generation; $NH_4H_2PO_4$ (ADP) and $ND_4D_2PO_4$ (DADP) crystals

PACS: 42.65.Dr, 42.65.Ky, 42.55.Rz, 42.70.Hj, 42.55.Ye

1. Introduction

Among practical electrooptic crystals and crystals for optical harmonic generation in the visible and UV spectral regions, as well as for optical parametric amplifiers in pettawatt-level solid-state laser systems the potassium dihydrogen phosphate KH_2PO_4 (KDP) and its deuterated analoque KD_2PO_4 hold a special place (see, e.g. [1]). These tetragonal phosphates and their numerous isomorphs comprise an important class of hydrogen-bonded crystals whose physical properties have been subjects of

* Corresponding author: e-mail: kaminalex@mail.ru

Crystal	SRS	SHG	THG	Self-TSRS [a]	Self-SFM (SRS) [b]	OPO [c]	OR [d]
$NH_4H_2PO_4$ (ADP)	+	+	+		+	+	+
$ND_4D_2PO_4$ (DADP) [e]	+	+	+		+		
KH_2PO_4 (KDP)	+	+		+		+	+
KD_2PO_4(DKDP) [e]	+	+		+		+	+
RbH_2PO_4	+	+					

[a] Self-TSRS, i.e. the self-transverse SRS from THG (see e.g. [8]).
[b] Self-SFM (SRS), i.e. self-sum-frequency mixing from the arising SRS lasing components and pumping radiation.
[c] OPO is the optical parametric oscillation (amplification).
[d] OR is the optical rectification.
[e] Deuterium concentration C_D = (95–97) at.%.

Table 1 Some effects of $\chi^{(3)}$- and $\chi^{(2)}$-nonlinear-laser generation in tetragonal crystals of KDP family

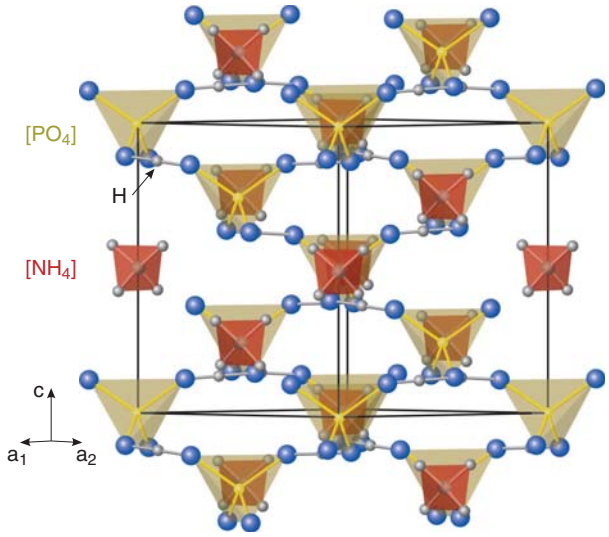

Figure 1 (online color at www.lphys.org) Plot of the crystal structure of $NH_4H_2PO_4$ [PO_4] and [NH_4] groups are marked with yellow and red tetrahedra, correspondingly

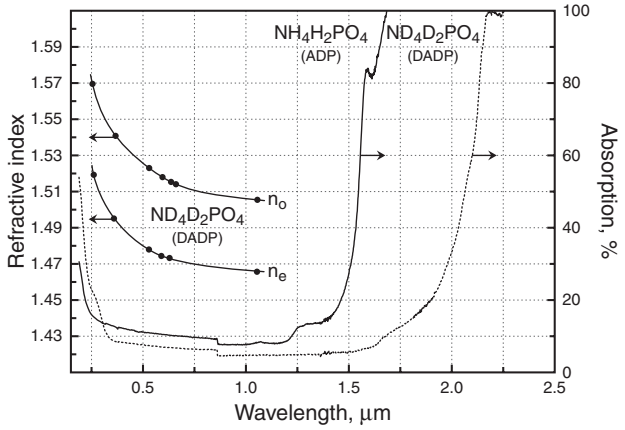

Figure 2 Room-temperature optical transmission spectra in the range from vacuum UV to near-IR of tetragonal $NH_4H_2PO_4$ and $ND_4D_2PO_4$ single crystals recorded with ≈ 1.5-mm plates without antireflection coating, and wavelength dispersion of refractive indices (see Table 2) of $ND_4D_2PO_4$ single crystal

extensive investigations (see, e.g. [2]). The $NH_4H_2PO_4$ (ADP) and $ND_4D_2PO_4$ (DAPD) are a well-known representatives of this phosphate family offering satisfactory linear and $\chi^{(2)}$-nonlinear optical properties in the UV spectral region [3,4]. Therefore, beside their nonlinear-laser potential which is indicated in Table 1, they were used also to get laser radiation with wavelengths shorted than 0.3 μm by second harmonic generation (SHG) and by sum-frequency mixing (see, e.g. [5], as well as Table 4.21 from [3]). It should be particularly emphasized here that KDP and ADP were the first crystals in which was realized the phase-matchable SHG [6]. These crystals are known as piezoelectric materials for ultrasonic technique as well (see e.g. [7]). The research reported in this work was performed within the context of an investigation of another nonlinear-laser properties of the $NH_4H_2PO_4$ (ammonium dihydrogen phosphate) and $ND_4D_2PO_4$ (deuterated ammonium dihydrogen phosphate) single crystals, namely stimulated Raman scattering (SRS), Stokes and anti-Stokes comb generation, third harmonic generation (THG) related to their $\chi^{(3)}$-nonlinearity, as well as cascaded $\chi^{(3)} \leftrightarrow \chi^{(2)}$ lasing in the visible and UV spectral ranges.

2. Crystals for experiments

Relatively large $NH_4H_2PO_4$ and $ND_4D_2PO_4$ single crystals of sufficient good optical quality have been grown from aqueous solutions using controlled lowering temperature at a growth velocity of about 1 mm/day (see e.g. [2]). The aqueous solution of $ND_4D_2PO_4$ was prepared recrystallizations in D_2O (heavy water). The deuteration

Characteristic	$NH_4H_2PO_4$	$ND_4D_2PO_4$
Space group	$D_{2d}^{12} - I\bar{4}2d$ [a] (No. 122)	
Unit cell parameters, Å [9]	$a = b = 7.4991(4)$, $c = 7.5493(12)$ (see Fig. 1)	$a = b = 7.5193(9)$, $c = 7.5400(19)$
Formula units per primitive cell	$Z^{Br} = 2$	
Temperature of phase transition (Curie temperature), K [10]	$T_C \approx 148$	$T_C \approx 242$
Density, g cm^{-3}	≈ 1.8	≈ 1.88
Method of crystal growth	Slow evaporation from an aqueous solution (see e.g. [2,11]), crystals commercially available [4]	
Hardness (Mhos scale)	1–2 [3,12]	
Optical character	Negative uniaxial ($n_o > n_e$)	
Optical transparency range, μm [b]	$\approx 0.18 - \approx 1.8$	$\approx 1.9 - \approx 2.3$
Thermal conductivity, W m^{-1} K^{-1}	0.7($\|c$−axis); 1.25 ($\perp c$−axis)	
Thermal expansion coefficients, 10^{-6}K^{-1} [c]	4.2 ($\|c$−axis); 32 ($\perp c$−axis)	
Piezoelectric coefficients, 10^{12} C N^{-1} [4]	$d_{14} = 1.3$; $d_{36} = 48$	$d_{14} = 10$; $d_{36} = 75$
Piezooptic constants [d] [4,13]	$p_{11} = 0.319$; $p_{12} = 0.277$; $p_{13} = 0.169$; $p_{31} = 0.197$; $p_{33} = 0.167$; $p_{44} = -0.058$; $p_{66} = -0.091$	
Elastic constants, 10^{10} N m^{-2} [4,13]	$c_{11} = 7.57$; $c_{12} = -2.43$; $c_{13} = 1.30$; $c_{33} = 2.96$; $c_{44} = 0.87$; $c_{66} = 0.61$	$c_{11} = 6.28$; $c_{12} = 0.395$; $c_{13} = 1.74$; $c_{33} = 3.18$; $c_{44} = 0.909$; $c_{66} = 0.61$
Electromechanical coupling factor	$k_{14} = 0.006$; $k_{36} = 0.33$[4]	
Linear electrooptic coefficients, 10^{-12} m V^{-1} for $\lambda = 0.633$ μm [1,14]	$r_{63}^T = -8.5$; $r_{41}^T = 24.5$; $r_{63}^S = 5.5$	$r_{63}^T = 11.9$
Nonlinearity	$\chi^{(2)}$ and $\chi^{(3)}$	
Nonlinear coefficient for SHG, 10^{-12} m V^{-1}	$d_{36} \approx 0.59$ [e] $d_{36} \approx 0.56$ [f]	$d_{36} \approx 0.52$ [e]
Refractive index	Sellmeier equations [g]	see Fig. 2 [h]
SHG phase-matching angles for $\lambda = 1.06$ μm	$\theta_{pm}^{oo-e} \approx 42°$; $\theta_{pm}^{oe-e} \approx 62°$	
Two-photon absorption coefficient, 10^{-6} cm MW^{-1}	$\beta = 6.8$ [i]	
Third-order nonlinear optical coefficients, 10^{20} m^2 V^{-2} [j]	$C_{11} = 0.0104$; $C_{18} = 0.0098$	
Laser-induced bulk-damage threshold, 10^{12} W m^{-2}	$I_{thr} \approx 5$ [k]	
Verdet constant, rad T^{-1} m^{-1}	$V \approx 251$ [l]	
Phonon spectrum extension, cm^{-1} [m]	≈ 3240	≈ 2450
Energy of the SRS-promoting vibration modes, cm^{-1}	$\omega_{SRS1} \approx 924$; $\omega_{SRS2} \approx 3160$	$\omega_{SRS1} \approx 883$; $\omega_{SRS2} \approx 2150$; $\omega_{SRS3} \approx 2265$; $\omega_{SRS4} \approx 2240$
Linewidth of peak in spontaneous Raman scattering spectra related to the SRS-promoting vibration transition, cm^{-1}	$\Delta\nu_{R1} \approx 27$; $\Delta\nu_{R2} \approx 150$	$\Delta\nu_{R1} \approx 27$; $\Delta\nu_{R2} \approx 60$; $\Delta\nu_{R3} \approx 100$; $\Delta\nu_{R4} \approx 70$

[a] Paraelectric state, under Curie temperature these crystals undergo phase transition to antiferroelectric state with space group $D_2^4 - P2_12_12_1$ (No. 19).
[b] For ≈ 1-mm thick plates (see Fig. 2).
[c] Within temperature interval (–50°C to +50°C) [9], see also [7,15].
[d] For $\lambda = 0.589$ μm.
[e] For $\lambda = 0.6943$ μm [16].
[f] For $\lambda = 1.0582$ μm [17].
[g] Sellmeier equations (λ in μm) [18] (see also [19]): $n_o^2 = 2.302484 + \frac{0.0117089}{\lambda^2 - 0.01314486} - \frac{3.751806\lambda^2}{100 - 0.25\lambda^2}$, $n_e^2 = 2.163077 + \frac{0.0096703}{\lambda^2 - 0.0128447} - \frac{1.451540\lambda^2}{100 - 0.25\lambda^2}$.
[h] For crystal with $C_D \approx 95$ at.% [4].

n	Wavelength, μm						
	0.266	0.3547	0.532	0.5893	0.6328	0.6443	1.064
n_o	1.5701	1.5403	1.5211	1.51815	1.5163	1.5142	.5052
n_e	1.5191	1.4942	1.4776	1.4751	1.47365	1.4719	1.4658

[i] For 2-cm long sample using THG of picosecond Nd^{3+}:$Y_3Al_5O_{12}$ laser at $\lambda \approx 0.355$ μm, accuracy of measurements was ± 35% [20].
[j] For ($-3\omega;\omega,\omega,\omega$) nonlinear optical process at $\lambda = 1.06$ μm [21].
[k] For 60-ns pulse radiation at $\lambda \approx 1.06$ μm [22], for other experimental conditions see also [3].
[l] At $\lambda = 0.6328$ μm [23].
[m] From spontaneous Raman scattering spectra, see Fig. 8 and [24].

Table 2 Crystallographic and some physical properties of tetragonal $NH_4H_2PO_4$ and $ND_4D_2PO_4$ single crystals at room temperature (limit of probable error in parentheses). Most of given data from [3,4]

Pumping condition		$\chi^{(3)}$- and $\chi^{(2)}$-lasing component			SRS-promoting modes, cm^{-1}			
λ_f, μm	Excitation geometry [a]	Wavelength, μm [b]	Line	Lasing attribution	ω_{SRS1}	ω_{SRS2}	ω_{SRS3}	ω_{SRS4}
$NH_4H_2PO_4$								
1.06415	*z(xx)z* (see Fig. 4)	0.3547	λ_{THG}	$3\omega_{f1}$				
		0.3667	λ_{SFM}	$2\omega_{f1}+\omega_{St1-1}$	$\approx$924			
		0.4135	ASt_{16-1}	$\omega_{f1}+16\omega_{SRS1}$	$\approx$924			
		0.4300	ASt_{15-1}	$\omega_{f1}+15\omega_{SRS1}$	$\approx$924			
		0.4477	ASt_{14-1}	$\omega_{f1}+14\omega_{SRS1}$	$\approx$924			
		0.4671	ASt_{13-1}	$\omega_{f1}+13\omega_{SRS1}$	$\approx$924			
		0.4882	ASt_{12-1}	$\omega_{f1}+12\omega_{SRS1}$	$\approx$924			
		0.5112	ASt_{11-1}	$\omega_{f1}+11\omega_{SRS1}$	$\approx$924			
		0.53207	λ_{SHG}	$2\omega_{f1}$	–	–	–	–
		0.5366	ASt_{10-1}	$\omega_{f1}+10\omega_{SRS1}$	$\approx$924			
		0.5596	λ_{SFM}	$\omega_{f1}+\omega_{St1-1}$	$\approx$924			
		0.5645	ASt_{9-1}	$\omega_{f1}+9\omega_{SRS1}$	$\approx$924			
		0.5956	ASt_{8-1}	$\omega_{f1}+8\omega_{SRS1}$	$\approx$924			
		0.6303	ASt_{7-1}	$\omega_{f1}+7\omega_{SRS1}$	$\approx$924			
		0.6693	ASt_{6-1}	$\omega_{f1}+6\omega_{SRS1}$	$\approx$924			
		0.7134	ASt_{5-1}	$\omega_{f1}+5\omega_{SRS1}$	$\approx$924			
		0.7638	ASt_{4-1}	$\omega_{f1}+4\omega_{SRS1}$	$\approx$924			
		0.8217	ASt_{3-1}	$\omega_{f1}+3\omega_{SRS1}$	$\approx$924			
		0.8893	ASt_{2-1}	$\omega_{f1}+2\omega_{SRS1}$	$\approx$924			
		0.9689	ASt_{1-1}	$\omega_{f1}+\omega_{SRS1}$	$\approx$924			
		1.06415	λ_{f1}	ω_{f1}	–	–	–	–
		1.1802	St_{1-1}	$\omega_{f1}-\omega_{SRS1}$	$\approx$924			
		1.3247	St_{2-1}	$\omega_{f1}-2\omega_{SRS1}$	$\approx$924			
		1.5094	St_{3-1}	$\omega_{f1}-3\omega_{SRS1}$	$\approx$924			
0.53207	*z(∠xy≈45°)z* (see Fig. 6a)	0.4109	ASt_{6-1}	$\omega_{f2}+6\omega_{SRS1}$	$\approx$924			
		0.4271	ASt_{5-1}	$\omega_{f2}+5\omega_{SRS1}$	$\approx$924			
		0.4446	ASt_{4-1}	$\omega_{f2}+4\omega_{SRS1}$	$\approx$924			
		0.4637	ASt_{3-1}	$\omega_{f2}+3\omega_{SRS1}$	$\approx$924			
		0.4844	ASt_{2-1}	$\omega_{f2}+2\omega_{SRS1}$	$\approx$924			
		0.5071	ASt_{1-1}	$\omega_{f2}+\omega_{SRS1}$	$\approx$924			
		0.53207	λ_{f2}	ω_{f2}	–	–	–	–
		0.5596	St_{1-1}	$\omega_{f2}-\omega_{SRS1}$	$\approx$924			
		0.5901	St_{2-1}	$\omega_{f2}-2\omega_{SRS1}$	$\approx$924			
		0.6241	St_{3-1}	$\omega_{f2}-3\omega_{SRS1}$	$\approx$924			
		0.6396	St_{1-2}	$\omega_{f2}-\omega_{SRS2}$		$\approx$3160		
		0.6623	St_{4-1}	$\omega_{f2}-4\omega_{SRS1}$	$\approx$924			
0.53207	*y(≈z≈z)y* (see Fig. 6b)	0.53207	λ_{f2}	ω_{f2}	–	–	–	–
		0.6396	St_{1-2}	$\omega_{f2}-\omega_{SRS2}$		$\approx$3160		
0.53207	*z(xx)z* (see Fig. 6c)	0.4109	ASt_{6-1}	$\omega_{f2}+6\omega_{SRS1}$	$\approx$924			
		0.4271	ASt_{5-1}	$\omega_{f2}+5\omega_{SRS1}$	$\approx$924			
		0.4446	ASt_{4-1}	$\omega_{f2}+4\omega_{SRS1}$	$\approx$924			
		0.4637	ASt_{3-1}	$\omega_{f2}+3\omega_{SRS1}$	$\approx$924			
		0.4844	ASt_{2-1}	$\omega_{f2}+2\omega_{SRS1}$	$\approx$924			
		0.5071	ASt_{1-1}	$\omega_{f2}+\omega_{SRS1}$	$\approx$924			
		0.53207	λ_{f2}	ω_{f2}	–	–	–	–
		0.5596	St_{1-1}	$\omega_{f2}-\omega_{SRS1}$	$\approx$924			
		0.5901	St_{2-1}	$\omega_{f2}-2\omega_{SRS1}$	$\approx$924			
		0.6241	St_{3-1}	$\omega_{f2}-3\omega_{SRS1}$	$\approx$924			
		0.6623	St_{4-1}	$\omega_{f2}-4\omega_{SRS1}$	$\approx$924			
$ND_4D_2PO_4$								
1.06415	*z(xx)z* (see Fig. 5)	0.3547	λ_{THG}	$3\omega_{f1}$	–	–	–	–
		0.3662	λ_{SFM}	$2\omega_{f1}+\omega_{St1-1}$	$\approx$883			
		0.3954	ASt_{18-1}	$\omega_{f1}+18\omega_{SRS1}$	$\approx$883			
		0.4097	ASt_{17-1}	$\omega_{f1}+17\omega_{SRS1}$	$\approx$883			
		0.4251	ASt_{16-1}	$\omega_{f1}+16\omega_{SRS1}$	$\approx$883			
		0.4416	ASt_{15-1}	$\omega_{f1}+15\omega_{SRS1}$	$\approx$883			

Pumping condition		$\chi^{(3)}$- and $\chi^{(2)}$-lasing component			SRS-promoting modes, cm^{-1}			
λ_f, μm	Excitation geometry [a]	Wavelength, μm [b]	Line	Lasing attribution	ω_{SRS1}	ω_{SRS2}	ω_{SRS3}	ω_{SRS4}
		0.4596	ASt_{14-1}	ω_{f1} + 14ω_{SRS1}	≈883			
		0.4790	ASt_{13-1}	ω_{f1} + 13ω_{SRS1}	≈883			
		0.5002	ASt_{12-1}	ω_{f1} + 12ω_{SRS1}	≈883			
		0.5233	ASt_{11-1}	ω_{f1} + 11ω_{SRS1}	≈883			
		0.53207	λ_{SHG}	$2\omega_{f1}$	–	–	–	–
		0.5486	ASt_{10-1}	ω_{f1} + 10ω_{SRS1}	≈883			
		0.5583	λ_{SFM}	$\omega_{f1} + \omega_{St1-1}$	≈883			
		0.5766	ASt_{9-1}	ω_{f1} + 9ω_{SRS1}	≈883			
		0.6074	ASt_{8-1}	ω_{f1} + 8ω_{SRS1}	≈883			
		0.6419	ASt_{7-1}	ω_{f1} + 7ω_{SRS1}	≈883			
		0.6805	ASt_{6-1}	ω_{f1} + 6ω_{SRS1}	≈883			
		0.7240	ASt_{5-1}	ω_{f1} + 5ω_{SRS1}	≈883			
		0.7734	ASt_{4-1}	ω_{f1} + 4ω_{SRS1}	≈883			
		0.8301	ASt_{3-1}	ω_{f1} + 3ω_{SRS1}	≈883			
		0.8958	ASt_{2-1}	ω_{f1} + 2ω_{SRS1}	≈883			
		0.9728	ASt_{1-1}	$\omega_{f1} + \omega_{SRS1}$	≈883			
		1.06415	λ_{f1}	ω_{f1}	–	–	–	–
		1.1745	St_{1-1}	$\omega_{f1} - \omega_{SRS1}$	≈883			
		1.3104	St_{2-1}	ω_{f1} − 2ω_{SRS1}	≈883			
		1.4819	St_{3-1}	ω_{f1} − 3ω_{SRS1}	≈883			
0.53207	*z(∠xy≈45°)z* (see Fig. 7a)	0.4309	ASt_{5-1}	ω_{f2} + 5ω_{SRS1}	≈883			
		0.4479	ASt_{4-1}	ω_{f2} + 4ω_{SRS1}	≈883			
		0.4663	ASt_{3-1}	ω_{f2} + 3ω_{SRS1}	≈883			
		0.4864	ASt_{2-1}	ω_{f2} + 2ω_{SRS1}	≈883			
		0.5082	ASt_{1-1}	$\omega_{f2} + \omega_{SRS1}$	≈883			
		0.53207	λ_{f2}	ω_{f2}	–	–	–	–
		0.5583	St_{1-1}	$\omega_{f2} - \omega_{SRS1}$	≈883			
		0.5873	St_{2-1}	ω_{f2} − 2ω_{SRS1}	≈883			
		0.6008	St_{1-2}	$\omega_{f2} - \omega_{SRS2}$		≈2150		
		0.6050	St_{1-3}	$\omega_{f2} - \omega_{SRS3}$			≈2265	
		0.6194	St_{3-1}	ω_{f2} − 3ω_{SRS1}	≈883			
		0.6552	St_{4-1}	ω_{f2} − 4ω_{SRS1}	≈883			
		0.6552	St_{4-1}	ω_{f2} − 4ω_{SRS1}	≈883			
0.53207	*y(≈z≈z)y* (see Fig. 7b)	0.4663	ASt_{3-1}	ω_{f2} + 3ω_{SRS1}	≈883			
		0.4864	ASt_{2-1}	ω_{f2} + 2ω_{SRS1}	≈883			
		0.5082	ASt_{1-1}	$\omega_{f2} + \omega_{SRS1}$	≈883			
		0.53207	λ_{f2}	ω_{f2}	–	–	–	–
		0.5583	St_{1-1}	$\omega_{f2} - \omega_{SRS1}$	≈883			
		0.5873	St_{2-1}	ω_{f2} − 2ω_{SRS1}	≈883			
		0.6041	St_{1-4}	$\omega_{f2} - \omega_{SRS4}$				≈2240
0.53207	*z(xx)z* (see Fig. 7c)	0.4309	ASt_{5-1}	ω_{f2} + 5ω_{SRS1}	≈883			
		0.4479	ASt_{4-1}	ω_{f2} + 4ω_{SRS1}	≈883			
		0.4663	ASt_{3-1}	ω_{f2} + 3ω_{SRS1}	≈883			
		0.4864	ASt_{2-1}	ω_{f2} + 2ω_{SRS1}	≈883			
		0.5082	ASt_{1-1}	$\omega_{f2} + \omega_{SRS1}$	≈883			
		0.53207	λ_{f2}	ω_{f2}	–	–	–	–
		0.5583	St_{1-1}	$\omega_{f2} - \omega_{SRS1}$	≈883			
		0.5873	St_{2-1}	ω_{f2} − 2ω_{SRS1}	≈883			
		0.6194	St_{3-1}	ω_{f2} − 3ω_{SRS1}	≈883			
		0.6552	St_{4-1}	ω_{f2} − 4ω_{SRS1}	≈883			

[a] Notation is used by analogy to [26], here are also $x \| a$, $y \| b$, and $z \| c$. The letters between the parentheses are (from left to right) the polarization of the pumping and laser scattering emission, respectively, while the ones to the left and the right of the parentheses are the pump and scatter emission directions, respectively. In the case of *y(≈z≈z)y* (see Fig. 6b and Fig. 7b) the polarization direction for pump and scatter emissions was approximately parallel to z-axis, in other case of *z(∠xy≈ 45°)z* (see Fig. 6a and Fig. 7a) the polarization for both emissions was directed approximately between x and y axes.

[b] Measurement accuracy is ± 0.0003 μm.

Table 3 Spectral composition of $\chi^{(3)}$- and $\chi^{(2)}$-nonlinear lasing at room temperature in tetragonal $NH_4H_2PO_4$ and $ND_4D_2PO_4$ single crystals with picosecond Nd^{3+}:$Y_3Al_5O_{12}$-laser pumping at λ_{f1} = 1.06415 μm and λ_{f2} = 0.53207 μm wavelengths

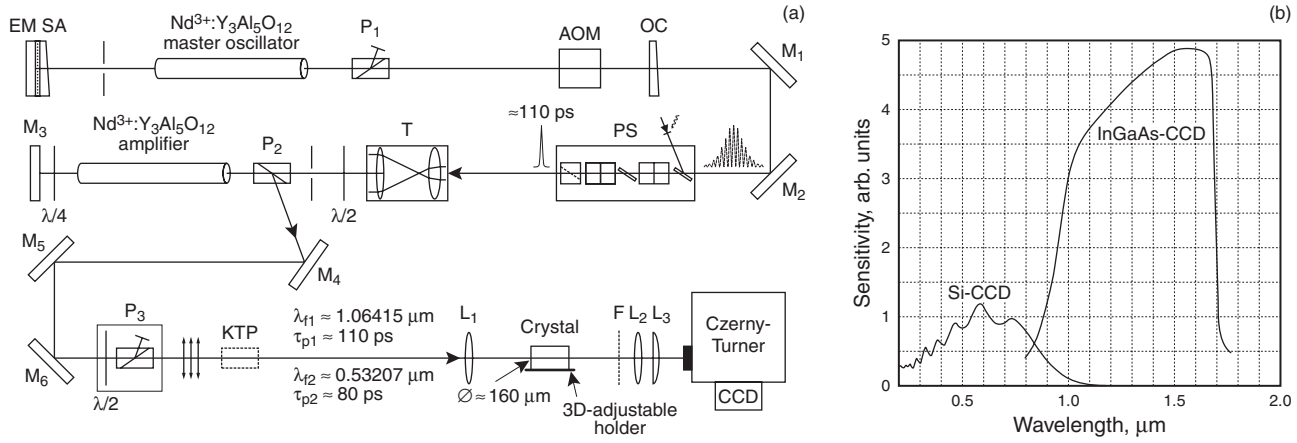

Figure 3 (a) – schematic diagram of the experimental setup and (b) – spectral sensitivity of used Si- and InGaAs-CCD sensors (data from Hamamatsu catalog)

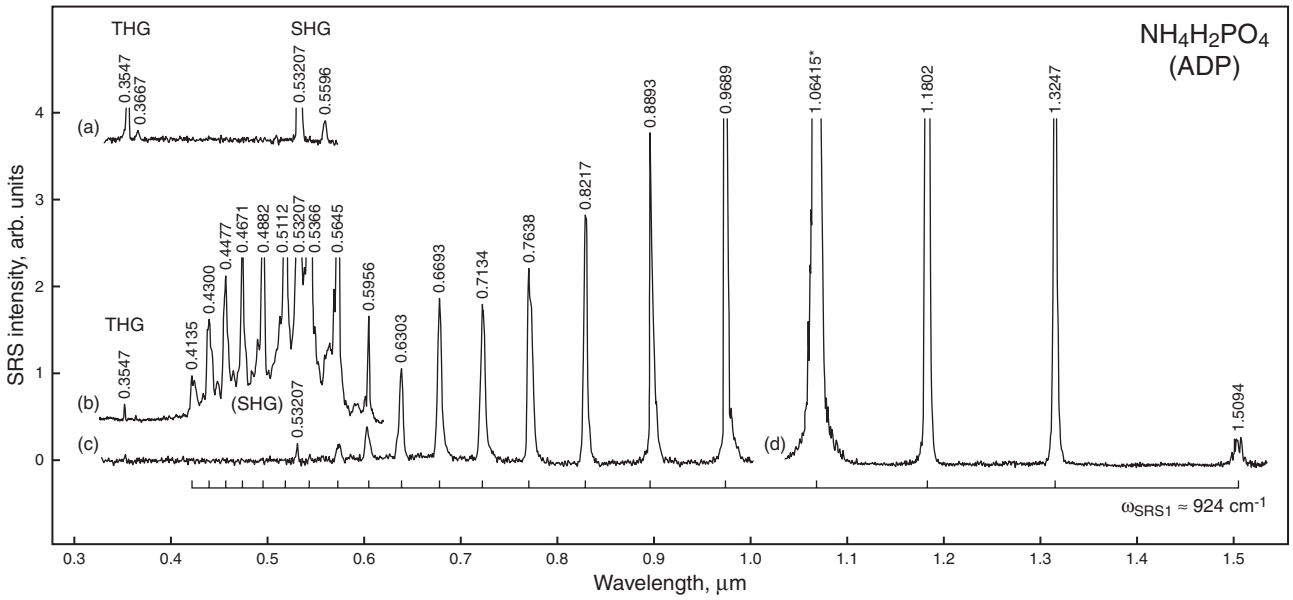

Figure 4 Room-temperature SRS and RFWM spectra tetragonal $NH_4H_2PO_4$ crystal recorded in pumping geometry *z(xx)z* with picosecond excitation at $\lambda_{f1} = 1.06415$ μm wavelength. Wavelengths of all lines (pump line is asterisked) are given in μm, and their spectral intensities are shown without correction for the spectral sensitivity of the used analyzing CSMA system with: Si-CCD (a-c) and InGaAs-CCD (d) array sensors. Spectra with cascaded self-frequency doubling (a,b) and self-frequency tripling (a,b) lasing components were obtained under special experimental condition (see text). The spacing of $\chi^{(3)}$-lasing components is multiple of SRS-promoting vibration mode ($\omega_{SRS1} \approx 924$ cm^{-1}) of crystal as indicated by the horizontal scale bracket

level of our $ND_4D_2PO_4$ crystals was estimated at 95–97%. For our stimulated and spontaneous Raman scattering, as well as optical experiments oriented samples in the form of bars (with active length 16–32 mm), cubs ($7\times8\times9$ mm^3), and $\approx$1.5-mm thick plates were fabricated. Their optical faces were polished plane-parallel but not anti-reflected coated. The crystallographic data and some known physical properties of these non-centrosymmetric $NH_4H_2PO_4$ and $ND_4D_2PO_4$ phosphates are compiled in Table 2.

3. Nonlinear $\chi^{(3)}$- and $\chi^{(2)}$-lasing

The room-temperature SRS measurements with $NH_4H_2PO_4$ and $ND_4D_2PO_4$ single crystals were carried

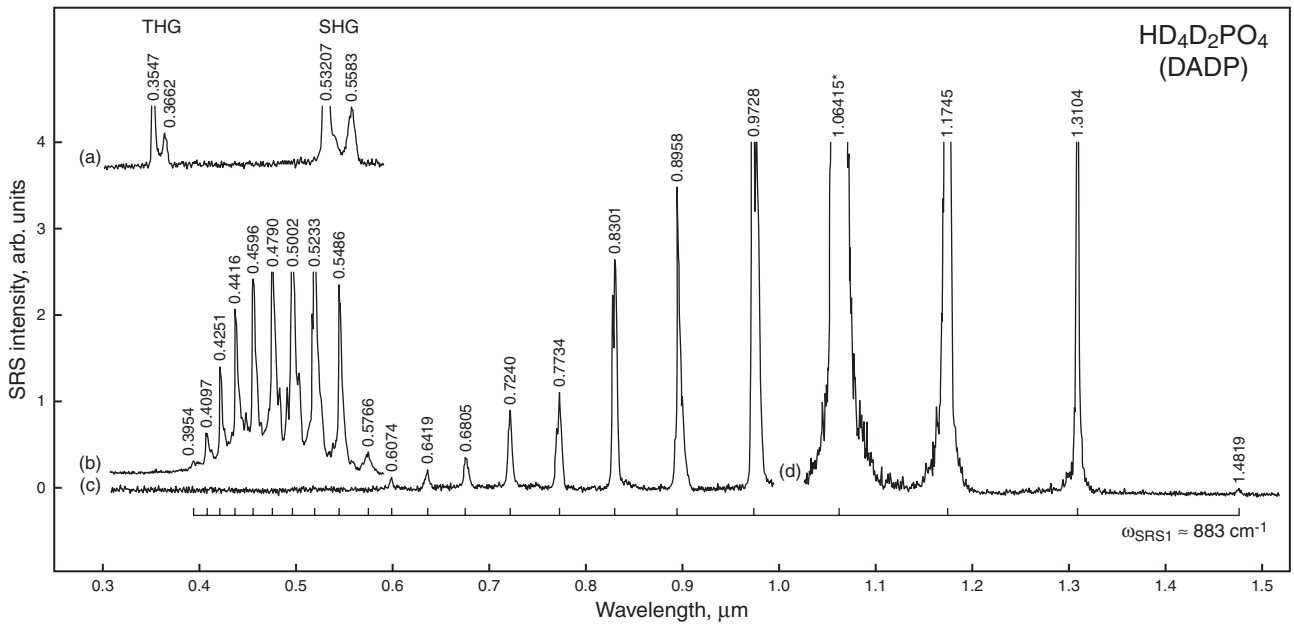

Figure 5 Room-temperature SRS and RFWM spectra of tetragonal $ND_4D_2PO_4$ crystal obtained in pumping geometry *z(xx)z* with picosecond excitation at $\lambda_{f1} = 1.06415$ μm wavelength. The spacing of $\chi^{(3)}$-lasing components is multiple of SRS-promoting vibration mode ($\omega_{SRS1} \approx 883$ cm^{-1}) of crystal as indicated by the horizontal scale bracket. Notations as in Fig. 4

out using a single-pass (cavity-free) excitation geometry with two-wavelength home-made Xe-flashlamp-pumped piscosecond Nd^{3+}:$Y_3Al_5O_{12}$ laser with $\approx$25%-efficient external $KTiOPO_4$ (KTP) doubler as a pumping source (schematic diagram of used experimental setup see in Fig. 3a). As may be seen, our laser is designed in a MOPA-scheme consisting of an actively-passively mode-locked oscillator and a double-pass amplifier. For passive pulse shortening and stabilization a saturable absorber liquid (SA) circulates through a cuvette placed directly in front of the resonator end-mirror (EM). In combination with an acousto-optic modulator (AOM) an output pulse train with the energy of about 2 mJ and single pulse duration of $\tau_{p1} \approx 110$ ps at λ_{f1} =1.06415 μm wavelength (main inter-Stark transition of the $^4F_{3/2} \rightarrow {}^4I_{11/2}$ laser channel of Nd^{3+} activators [25]) is emitted. A pulse slicer (PS) only transmits the central single pulse by optical triggering of two double-Pockels-cells placed between three polarizers in $\pi-\pi-\sigma$ orientation. The energy of the resulting single pulse is about 200 μJ. In order to increase this pulse up to than 40 mJ, Nd^{3+}:$Y_3Al_5O_{12}$ amplifier in a double-pass alignment is designed. To widen the beam diameter to 4.5 mm to adopt it to the amplifier Nd^{3+}:$Y_3Al_5O_{12}$ rod a telescope is used. After the second pass through the λ/4-wave plate and the laser rod the beam polarization is rotated by ninety degrees and extracted with a Glan-laser polarizer (P_2). A λ/2-wave plate along with another Glan-laser polarizer (P_3) is inserted to attenuate the energy to the required value keeping the plane of polarization parallel to the optical table. In this case the IR-pump beam is suppressed behind the doubler and before entering the investigated crystal by a Schott BG39 glass-filter with a transmission of 0.015% at $\lambda_{f1} = 1.06415$ μm wavelength. The same filter is used to suppress the IR-pump beam, as well as the deep red and intense IR scattering components before the monochromator to investigate week lasing emission in the UV-region. The nearly Gaussian pump beam is then focused into the SRS-active crystal with a spherical plane-convex lens L_1 (f = 250 mm), resulting in a beam waist diameter of about $\varnothing \approx 160\,\mu$m. Alignment of investigated sample to the required orientation is possible by three-axis translation and rotation using a customized 3D-adjustable holder. A spherical bi-convex quartz lens L_2 ($\approx$50 mm diameter, f = 100 mm) and a plane-convex cylindrical quartz lens L_3 (50×50 mm^2, f = 100 mm) are used to collimate the lasing scattering emission into the entrance slit of the monochromator. The spectral composition of the multi-component nonlinear $\chi^{(3)}$- and $\chi^{(2)}$-lasing in our phosphate crystals studied was measured with a spectrometric multi-channel analyzer system (CSMA) on the base a scanning grating monochromator in Czerny-Turned arrangement (McPherson Model 270, dispersion of 6.8 Å/pixel with a grating of 150 lines/mm) that was equipped with two Hamamatsu linear image sensors Si-CCD (S3923-1024Q with 1023 pixels) and InGaAs-CCD (G9204-512D with 512 pixels) which provide good enough sensitivity in UV, visible, and near-IR rangers (see Fig. 3b).

Several typical ($\chi^{(3)}$ and $\chi^{(2)}$) lasing spectra of $NH_4H_2PO_4$ and $ND_4D_2PO_4$ crystals recorded in differ-

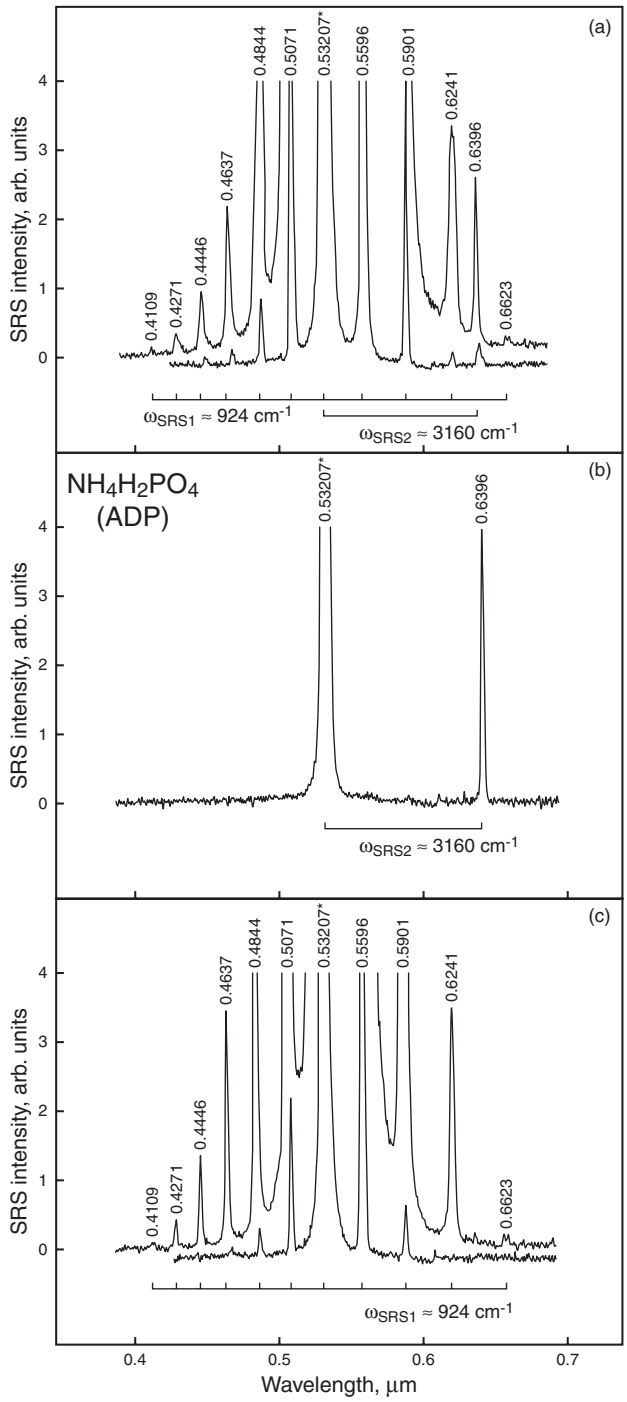

Figure 6 Room-temperature SRS and RFWM spectra of tetragonal $NH_4H_2PO_4$ crystal obtained under picosecond excitation at $\lambda_{f2} = 0.53207$ μm wavelength in pumping geometry: (a) $z(\angle xy \approx 45^\circ)z$, (b) $y(\approx z \approx z)y$, and (c) $z(xx)z$ (see notes of Table 3). The spacing of $\chi^{(3)}$-lasing components is multiple of SRS-promoting vibration modes $\omega_{SRS1} \approx 924$ cm^{-1} (a,c) and $\omega_{SRS2} \approx 3160$ cm^{-1} (a,b) of crystal as indicated by the horizontal scale bracket. Notations as in Fig. 4

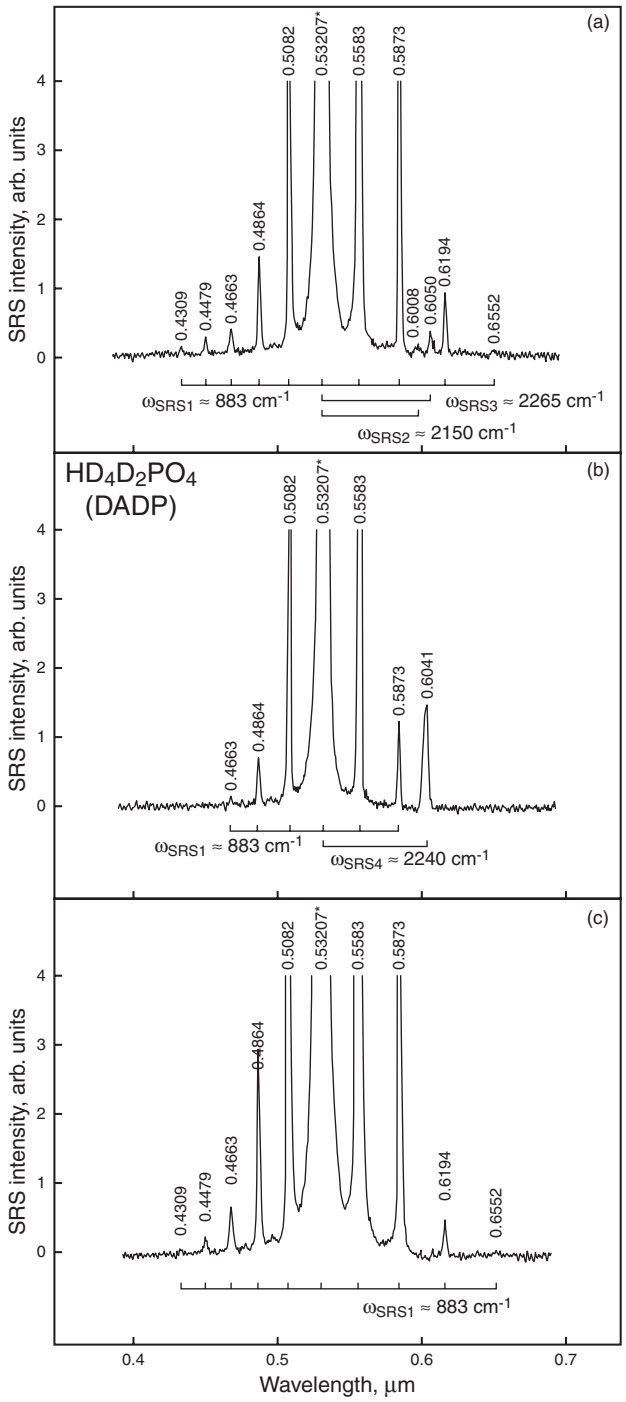

Figure 7 Room-temperature SRS and RFWM spectra of tetragonal $NH_4H_2PO_4$ crystal obtained under picosecond excitation at $\lambda_{f2} = 0.53207$ μm wavelength in pumping geometry: (a) $z(\angle xy \approx 45^\circ)z$, (b) $y(\approx z \approx z)y$, and (c) $z(xx)z$ (see notes of Table 3). The spacing of $\chi^{(3)}$-lasing components is multiple of SRS-promoting vibration modes $\omega_{SRS1} \approx 883$ cm^{-1} (a,b,c), $\omega_{SRS2} \approx 2150$ cm^{-1} (a), $\omega_{SRS3} \approx 2265$ cm^{-1} (a), $\omega_{SRS4} \approx 2240$ cm^{-1} (b) of crystal as indicated by the horizontal scale bracket. Notation as in Fig. 4

ent excitation geometries and results of their analysis are shown in Fig. 4 – Fig. 7 and summarized in Table 3. These data evidenced that we can to obtain almost two-octave Stokes and anti-Stokes combs for both crystals under excitation at $\lambda_{f1} = 1.06415$ μm wavelength (20 components from 1.5094 μm till 0.4135 μm for $NH_4H_2PO_4$ see Fig. 4, and 22 components from 1.4819 μm till 0.3954 μm for $ND_4D_2PO_4$ see Fig. 5, including pumping line for both cases). Carried out experiments showed that in non-centrosymmetric $NH_4H_2PO_4$ and $ND_4D_2PO_4$ crystals under selected pumping conditions could proceed several nonlinear-lasing $\chi^{(3)}$- and $\chi^{(2)}$-effects. In particular, there are non-phase-matchable SHG and THG, and relating to them the cascaded self-sum-frequency mixing processes. To clear supervision of these spectra we significant decreased unwanted (saturated) influence of strong one-micron pumping and several first Stokes and anti-Stokes bands emission on recording characteristics of the used CSMA system. For this aim we used catalog optical filters and other known experimental contrivances which permit to enhance the real sensitivity of its Si-CCD sensor in the visible and UV spectral regions. Obtained spectra are shown in Fig. 4a, Fig.4 b, Fig. 5a, and Fig. 5b and results of their interpretation are given in Table 3. Among other things under pumping at $\lambda_{f1} = 1.06415$ μm wavelength we have recorded also in both crystals visible to the naked one- or two-conical Cherenkov-type SHG for all investigated excitation geometries. More details of the observed new nonlinear optical effects in $NH_4H_2PO_4$ and $ND_4D_2PO_4$ phospates will be published in a further paper. It should be noted here that Cherenkov type SHG was observed also in non-centrosymmetric crystals – in the trigonal β-$LaBGeO_5$ [27] and tetragonal $Li_2B_4O_7$ [28] borates. It is felt that such nonlinear-laser behavior is features for all KDP-family crystals in the tetragonal D_{2d}^{12}-phase. At least this confirm also numerous results of nonlinear-laser experiments with crystals which listed in Table 1 and other data on KDP-family crystals given in [2–4].

We can carried out also rough experimental estimation of steady-state (ss) Raman gain coefficients for first Stokes lasing components ($g_{ssR}^{St_{1-1}}$) of $NH_4H_2PO_4$ and $ND_4D_2PO_4$ crystals because our pumping conditions are in accordance with this $\chi^{(3)}$-nonlinear-laser generation regime $\tau_p \gg T_2 = (\pi \Delta\nu_R)^{-1} \approx 0.4$ (here T_2 is the dephasing time of SRS-promoting phonon mode and $\Delta\nu_R$ is the linewidth of the Raman shifted line (see Table 2 and Fig. 8) related to the SRS-promoting vibration transition). For this aim we restored to sufficient tested method (see, e.g. [29]) based on the well-known ratio [30] $g_{ssR}^{St1-1} I_p^{thr} l_{SRS} \approx 30$ and comparative measurements under similar experimental arrangements of "threshold" pump intensity (I_p^{thr}) of the confidently detectable first-Stokes signal for $NH_4H_2PO_4$ (at $\lambda_{St1-1} = 1.1802$ μm, see Fig. 4) and $ND_4D_2PO_4$ (at $\lambda_{St1-1} = 1.1745$ μm, see Fig. 5) phosphates and for reference crystal $PbWO_4$ with known value of g_{ssR}^{St1} coefficient (at $\lambda_{St1} = 1.1770$ μm [31]) and with nearly the same SRS-active length (l_{SRS}). Carried out measurements showed that the first Stokes "threshold" intensity for reference tungstate was roughly 7 and 11 times less than for $NH_4H_2PO_4$ and $ND_4D_2PO_4$ phosphates, respectively. These data allow us to conclude that the desired g_{ssR}^{St1-1} coefficients not less than 0.44 cm GW^{-1} for $NH_4H_2PO_4$ and not less than 0.28 cm GW^{-1} for $ND_4D_2PO_4$ crystal. The activity of another recorded $\chi^{(3)}$-lasing in $NH_4H_2PO_4$ and $ND_4D_2PO_4$ crystals that connected with their high-frequency vibration modes is sufficiently low.

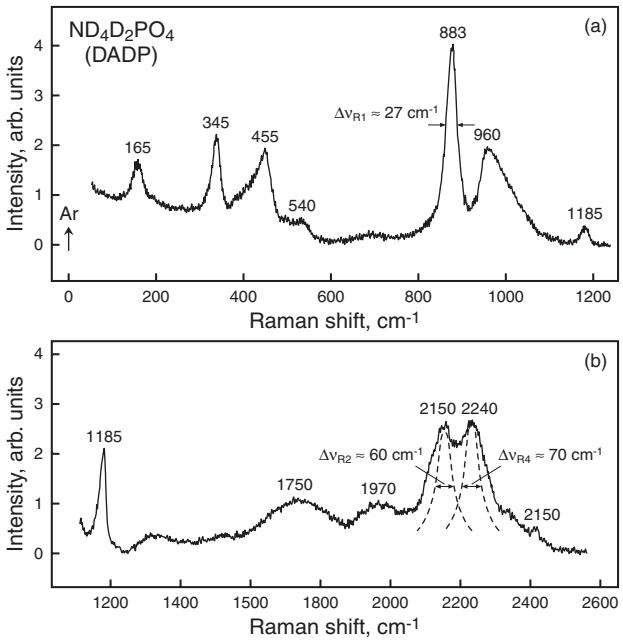

Figure 8 Room-temperature spontaneous Raman scattering spectrum of $ND_4D_2PO_4$ single crystal given in two fragments (a) from 0 till 1200 cm^{-1} and (b) from 1200 till 2600 cm^{-1} (modified spectrum of [24] which was recorded in scattering geometry *x(yy)z* under an Ar-ion laser excitation at 0.5145 μm wavelength). The frequency of some intense Raman shifted lines are given in cm^{-1}

Now briefly about vibration nature of strong SRS-promoting vibrational transitions of crystal studied. Its primitive D_{2d}^{12} cell contains two formula units, giving rise to $3NZ^{Br} = 72$ degree of vibration freedom that are distributed in accordance with the symmetry representations [32] (at $\mathbf{k} = 0$) as: $\Gamma_{72} = 7A_1 + 8A_2 + 9B_1 + 10B_2 + 19E$. Among them three acoustic modes are symmetry B_2 and E, eight A_2 symmetry modes are optically inactive. Otherwise species are the Raman active, among them ten B_2 and eighteen double degenerate E modes are also IR-active. Results of our preliminary analysis of recorded Raman spectra and rich literature data on vibration properties $NH_4H_2PO_4$ and $ND_4D_2PO_4$ crystals (see. e.g. [24,33] make possible to conclude that strong peaks at ≈ 924 cm^{-1} and ≈ 883 cm^{-1} wavenumbers which con-

nected with the SRS lasing effect, are due to the totally symmetric "breathing" $A_1(\nu_1)$-optical mode of tetrahedral PO_4^{-3} groups of these phosphates. According to [24,34] other SRS-active vibrations above 2000 cm^{-1} belong to internal stretching N-H(N-D) modes and H-H (D-D) bonds of $NH_4^+(ND_4^+)$ ions of studied phosphates.

4. Summary

We have conducted steady-state SRS experiments that open up new nonlinear-laser capabilities of two non-centrosymmetric $NH_4H_2PO_4$ and $ND_4D_2PO_4$ crystals which widely used in piezotechnics, electrooptic, and nonlinear optics. In particular, by one-micron picosecond pumping we excited and recorded almost two-octave multi-component their Stokes and anti-Stokes combs (contining: 20 wavelengths within 1.5094 μm and 0.4135 μm range for $NH_4H_2PO_4$ and 22 wavelengths within 1.4819 μm and 0.3954 μm for $ND_4D_2PO_4$ crystal) and cascaded nonlinear lasing $\chi^{(3)} \leftrightarrow \chi^{(2)}$ effects in UV and visible ranges that involve of non-phase-matched second and third harmonic emission of these phosphates. All the recorded SRS and multi-wave mixing component were identified and attributed to the SRS-active vibration transitions of studied crystals. The estimated appreciable values of first Stokes "one-micron" steady-state Raman gain coefficients indicate that ADP and DADP crystals could be classified as promising media for up- and down-Raman laser frequency converters. We think that the obtained experimental data of very spread Stokes and anti-Stokes combs lets us come closer to the synthesis of femtosecond optical waveforms. For this aim we plan to perform crossing two- or many-color pumping beams with frequency differences that are equal to SRS frequencies in $NH_4H_2PO_4$ and $ND_4D_2PO_4$ crystals.

Acknowledgements The research was supported in part by the Russian Foundation for Basic Research and the Program "Femtosecond physics and new optical materials" of the Presidium of Russian Academy of Sciences, as well as the Technical University of Berlin. One of us (A.A.K.) is grateful to the Alexander von Humboldt Foundation for the "Festkorperphysik" Research Prize, which allowed him to carried out SRS experiments in Institute of Optics and Atomic Physics of the Technical University of Berlin. All authors like to note that progress in the present work was made possible by cooperation with the Joint Open Laboratory for Laser Crystals and Precise Laser Systems. The authors thank also C. Scharfenorth, L.N. Rashkovich, and V.S. Gorelik for experimental help, councels and discussions.

References

[1] I.P. Kaminow and E.H. Turner, Appl. Opt. **5**, 1612 (1966); M.J. Weber (ed.), CRC Handbook of Optical Materials (CRC Press, Boca Raton, FL, 2003); S.M. Kulikov, V.A. Lebedev, G.P. Okutin, N.N. Rukavishnikov, and S.A. Sukharev, Proc. SPIE **3492**, 1009 (1998); V.V. Lozhkarev, G.I. Freidman, V.N. Ginzburg, E.V. Katin, E.A. Khazanov, A.V. Kirsanov, G.A. Luchinin, A.N. Mal'shakov, M.A. Martyanov, O.V. Palashov, A.K. Poteomkin, A.M. Sergeev, A.A. Shaykin, and I.V. Yakovlev, Laser Phys. Lett. **4**, 421 (2007).

[2] I.S. Rez, Sov. Phys. Usp. **10**, 759 (1968); M. Tokunaga, Ferroelectrics **1**, 195 (1970); L.N. Rashkovich, KDP Family Single Crystals (Adam Hilger, Bristol, Philadelphia, New-York, 1991).

[3] V.G. Dmitriev, G.G. Gurzadyan, and D.N. Nikogosyan, Handbook of Nonlinear Optical Crystals (Springer, Berlin, 1997).

[4] Landolt-Börnstein, Vol. III-16b (Springer, Berlin, 1987); Landolt-Börnstein, Group VIII: Advanced Materials and Technologies, Vol. 1, Laser Physics and Applications, Subvolume A: Laser Fundamentals, Part 1 (Springer, Berlin, 2005); Cleveland Crystals Catalog (www.clevelandcrystals.com) and their references.

[5] K. Kato, Opt. Commun. **13**, 361 (1975); G. Massey and J. Johnson, IEEE J. Quantum Electron. **12**, 721 (1976).

[6] J.A. Giordmaine, Phys. Rev. Lett. **8**, 19 (1962); P.D. Maker, R.W. Terhune, M. Nisenoff, and C.M. Savage, Phys. Rev. Lett. **8**, 21 (1962).

[7] W.P. Mason, Piezoelectric Crystals and Their Application to Ultrasonics (D. Van Nostrand, New York, 1950).

[8] V.N. Novikov, S.A. Belikov, S.A. Buiko, I.N. Voronich, D.G. Efimov, A.I. Zaretsky, G.G. Kochemasov, A.G. Kravchenko, S.M. Kulikov, V.A. Lebedev, G.P. Okutin, N.N. Rukavishnikov, and S.A. Sukharev, Proc. SPIE 3492, 1009 (1998).

[9] W.R. Cook, Jr., J. Appl. Phys. **38**, 1637 (1967).

[10] B.T. Matthias, Phys. Rev. **85**, 141 (1952).

[11] S.L. Wang, Z.S. Gao, Y.J. Fu, A.D. Duan, X. Sun, C.S. Fang, and X.Q. Wang, Cryst. Res. Technol. **38**, 941 (2003).

[12] M.J. Weber (ed.), CRC Handbook of Laser Science and Technology (CRC Press, Boca Raton, FL, 1995).

[13] R.S. Adhav, J. Acoust. Soc. Am. **43**, 835 (1968); T.S. Narasimhamurty, K. Veerabhadra Rao, and H.E. Pettersen, J. Mater. Sci. **8**, 577 (1973).

[14] R.O'B. Carpenter, J. Opt. Soc. Am. **40**, 225 (1950); J.H. Ott and T.R. Sliker, J. Opt. Soc. Am. **54**, 1442 (1964); I.P.Kaminov, An Introduction to Electrooptic Devices (Academic Press, New York, 1974).

[15] S. Haussühl, Z. Kristallogr. **120**, 401 (1964).

[16] V.S. Suvorov, A.S. Sonin, and I.S. Rez, JETP **26**, 33 (1968).

[17] R.C. Miller and A. Savage, Phys. Rev. **128**, 2175 (1962).

[18] G.R. Elion, Electro-Optics Handbook (Marcel Dekker Ltd., New York, 1979).

[19] D. Eimerl, Ferroelectrics **72**, 95 (1987); K.W. Kirby and L.G. DeShazer, J. Opt. Soc. Am. B **4**, 1072 (1987).

[20] P. Liu, W.L. Smith, H. Lotem, J.H. Bechtel, N. Bloembergen, and R.S. Adhav, Phys. Rev. B **17**, 4620 (1978).

[21] V.D. Volosov and E.V. Nilov, Opt. Spectrosc. (USSR) **21**, 39 (1966).

[22] C.C. Wang and E.L. Baardsen, Appl. Phys. Lett. **15**, 396 (1969).

[23] S. Haussühl and W. Effgen, Z. Kristallogr. **183**, 153 (1988).

[24] M. Kasahara, M. Tokunaga, and I. Tatsuzaki, J. Phys. Soc. Jpn. **55**, 367 (1986); I. Kanesaka and C. Watanabe, J. Raman Spectrosc. **29**, 153 (1998).

[25] A.A. Kaminskii, Zh. Eksp. Teor. Fiz. **51**, 49 (1966); A.A. Kaminskii, Laser Crystals, Their Physics and Properties (Springer, Berlin, 1980 and 1990).
[26] T.C. Damen, S.P.S. Porto, and B. Tell, Phys. Rev. **142**, 570 (1966).
[27] A.A. Kaminskii, H. Nishioka, K. Ueda, W. Odajiama, M. Tateno, K. Sasaki, and A.V. Butashin, Quantum Electron. **26**, 381 (1996).
[28] A.A. Kaminskii, L. Bohatý, P. Becker, J. Liebertz, H.J. Eichler, and H. Rhee, Laser Phys. Lett. **3**, 519 (2006).
[29] A.A. Kaminskii, H.J. Eichler, K. Ueda, N.V. Klassen, B.S. Redkin, L.E. Li, J. Findeisen, D. Jaque, J. García-Sole, J. Fernández, and R. Balda, Appl. Opt. **38**, 4533 (1999).
[30] Y.R. Shen, The Principles of Nonlinear Optics (Wiley, New York, 1984).
[31] A.A. Kaminskii, C.L. McCray, H.R. Lee, S.W. Lee, D.A. Temple, T.H. Chyba, W.D. Marsh, J.C. Barnes, A.N. Annanenkov, V.D. Legun, H.J. Eichler, G.M.A. Gad, and K. Ueda, Opt. Commun. **183**, 277 (2000).
[32] D.L. Rousseau, R.P. Bauman, and S.P.S. Porto, J. Raman Spectrosc. **10**, 253 (1981).
[33] H. Ratajczk, J. Mol. Struct. **3**, 27 (1969); T. Kawamura and A. Mitsuishi, Tech. Rep. of the Osaka Univ. **23**, 365 (1973); J.J. Kim and W.F. Sherman, Phys. Rev. B **36**, 5651 (1987).
[34] W.G. Fateley, N.T. McDevitt, and F.F. Bentley, Appl. Spectrosc. **25**, 155 (1971); K. Nakamoto, Infrared and Raman Spectra of Inorganic and Coordination Compounds (Wiley, New York, 1978); R.J.H. Clark and R.E. Hester, Advances in Infrared and Raman Spectrosopy (Wiley, New York, 1983).